

ARTICLE OPEN



Weather whiplash events in Europe and North Atlantic assessed as continental-scale atmospheric regime shifts

Jennifer A. Francis^{1✉}, Natasa Skific² and Zachary Zobel¹

The term “weather whiplash” describes abrupt transitions from one persistent weather regime to another substantially different one, such as from a frigid cold spell to anomalous warmth. Weather whiplash events (WWEs) are often highly disruptive to agriculture, ecosystems, infrastructure, and human activities. While no consistent definition exists, we identify WWEs based on substantial shifts in the continental-scale, upper-atmosphere circulation. As first demonstrated in our earlier study focused on the NE Pacific/North American region, a WWE is detected when one persistent, large-scale pattern in 500 hPa height anomalies shifts to another distinctly different one. Patterns are identified using self-organizing maps (SOMs), which create a matrix of representative patterns in the data. In the present study, we apply this approach to identify WWEs in the North Atlantic/European sector. We analyze the occurrence of WWEs originating with long-duration events (four or more days) in each pattern. A WWE is detected when the pattern two days following a long-duration event is substantially different, measured with distance thresholds internal to the matrix. Changes in WWE frequency, past and future, are assessed objectively based on reanalysis output and climate model simulations. We find that future changes under RCP 8.5 forcing exhibit distinct trends, especially in summer months, while those based on reanalysis are less clear. Patterns featuring positive height anomalies in high latitudes are projected to produce more WWEs in the future, while patterns exhibiting negative anomalies produce fewer. Shifts in temperature and precipitation extremes associated with these WWEs are diagnosed.

npj Climate and Atmospheric Science (2023)6:216; <https://doi.org/10.1038/s41612-023-00542-9>

INTRODUCTION

According to the World Meteorological Organization, temperatures in Europe have increased more than twice the global-average rate over the past 30 years—the fastest of any continent^{1,2}. Accompanying the heating has been a significant increase in both the number and intensity of extreme weather events and natural disasters³. Summer heat waves have become more frequent, widespread, and deadly^{2,4}. Europe’s winters have also become increasingly warm and dry; in 2022 alone, Italy, Spain, the UK and France all set new high-temperature records. Precipitation in the Mediterranean region during winter has declined by approximately 6 mm dec⁻¹ since 1901⁵, affecting agriculture, drinking water supplies, and energy production⁶. In addition to altered precipitation patterns, agriculture is also challenged by rising temperatures, extreme weather events that are becoming more frequent and intense, and abrupt changes in weather conditions, sometimes referred to as weather whiplash events^{7,8} (WWEs). These events are particularly disruptive when the initial anomalous conditions persist for days or weeks before the shift, and thus can be highly disruptive to infrastructure and ecosystems. Long-duration drought followed by heavy precipitation, for example, can damage crops. Orchards can be devastated by the arrival of a severe cold snap after a persistent early-spring warm spell. Prolonged summer heat waves and drought have also fueled wildland fires across Mediterranean Europe⁹, and if these conditions shift abruptly to a stormy pattern with intense rain, barren burn scars will absorb little moisture and raise the threat of flash flooding, which has been particularly pronounced in Greece in recent years¹⁰. Despite the damage caused by whiplash events, there has been little research focused on them and how they may change as the globe continues to warm. In this study, we aim to

shed light on the continental-scale atmospheric patterns across the North Atlantic and Europe that are most likely to initiate WWEs, the weather transitions associated with them, and how they may change in the future.

The present study builds on Francis et al. (2022, hereafter F22)¹ in which we demonstrated and applied an objective approach to diagnosing and tracking WWEs. As explained in F22, however, no consistent, quantitative, comprehensive definition of a WWE had existed. Some studies targeted large and rapid changes in air temperature^{11–13}, while others focused on shifts in precipitation regimes^{14–16}. (See F22 for a more detailed review of previous related studies.) The approach presented in F22 focuses on major shifts in persistent, continental-scale regimes rather than local changes in weather conditions. It objectively identifies long-duration atmospheric patterns in upper-level height surfaces as well as the transition to a new regime. Variations in these large-scale circulation patterns are indicative of shifting ridges and troughs in the jet stream, which in turn, create and steer the high and low sea-level pressure cells that dictate surface weather conditions, including winds, cloudiness, temperature, and precipitation. Thus, when a persistent, distinct circulation pattern shifts to another substantially different one, the weather also changes, often dramatically.

We use a neural network-based pattern recognition tool called Self-Organizing Maps (SOMs). Originally developed to diagnose images in the medical field¹⁷, SOMs have been applied to analyzing a wide range of atmospheric features and behaviors^{1,18} (and references therein). The tool not only identifies characteristic patterns in the data and presents the fields in intuitive, two-dimensional maps, but it can also reveal temporal changes in

¹Woodwell Climate Research Center, 149 Woods Hole Rd, Falmouth, MA 02540, USA. ²Department of Marine and Coastal Sciences, Rutgers University, 71 Dudley Rd, New Brunswick, NJ 08901, USA. ✉email: jfrancis@woodwellclimate.org

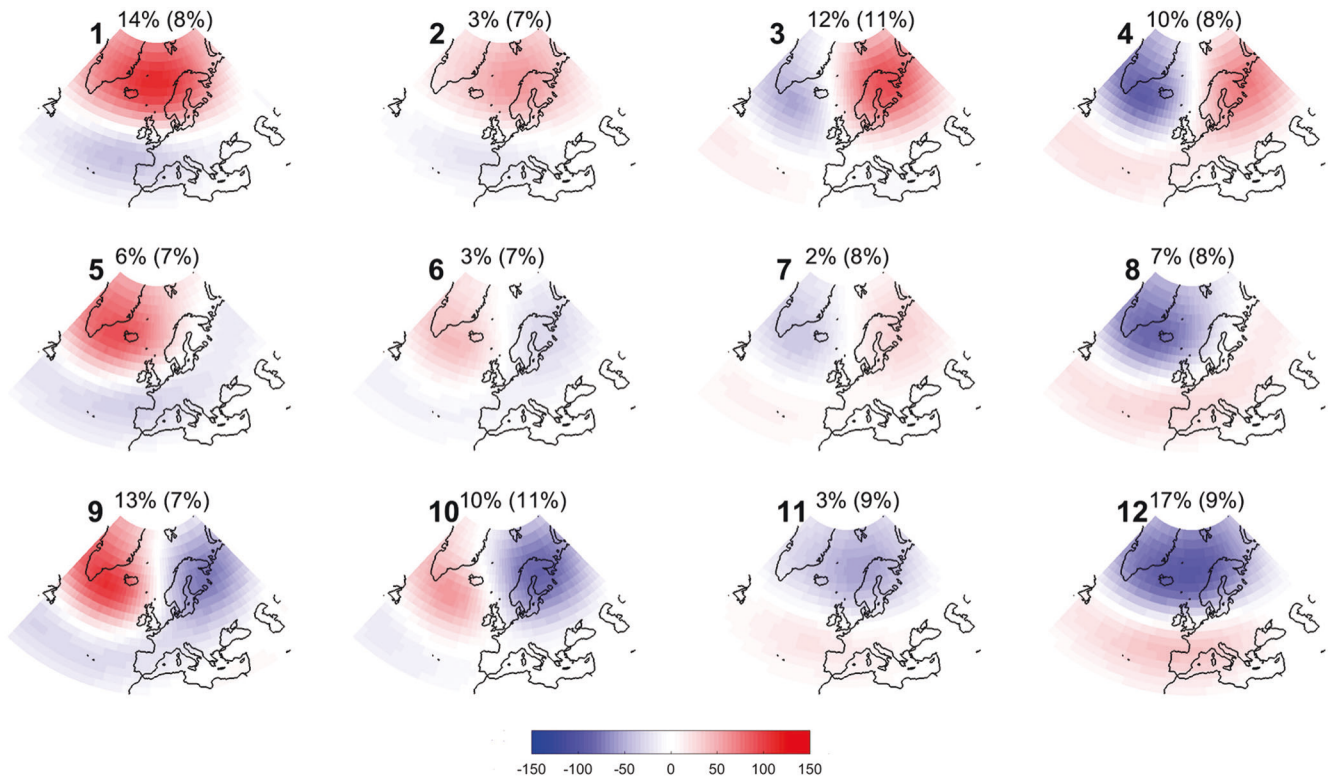


Fig. 1 The master SOM matrix. Representative patterns in daily 500-hPa geopotential height anomalies [m, shaded] for all months from 1948–2021 were calculated using Self-Organizing Maps. The domain covers 30°N–80°N and 60°W–60°E (midlatitude North Atlantic/Europe). Percentages indicate the frequency of occurrence of each node during winter (JFM) and summer (JAS; in parentheses). The numbers to the left of each node are for reference purposes. Height fields to generate the SOM were obtained from the NCEP/NCAR Reanalysis²⁰ (Kalnay et al.³¹).

pattern frequency as well as analyze other variables associated with those patterns.

The earlier work published in F22 demonstrated the approach by identifying and analyzing WWEs over the eastern North Pacific Ocean and North America. We defined WWEs as a shift from one persistent (longer than four consecutive days), large-scale pattern in 500 hPa height anomalies to another distinctly different pattern 1–2 days later, assessed using a quantitative distance metric. This definition eliminates confusion in the possible misidentification of WWEs caused by weather changes over short time scales owing to routine passages of synoptic features, such as fronts, discrete disturbances (e.g., squall lines, tropical storms), and abrupt temperature swings caused by local surface effects (e.g., the arrival of a sea breeze or downslope flow). The large-scale approach demonstrated in F22 has the advantage of focusing on regime shifts rather than local-scale abrupt changes. We further demonstrated that temperature and precipitation extremes associated with each pattern are useful tool for assessing the disruptive impacts of specific WWEs across the domain. Because SOMs can be applied to both reanalysis and climate-model output, we were able to analyze changes in WWE frequency over the past and future, as well as associate those changes with the patterns most likely to spawn the WWEs. While no significant changes in WWE frequency were found during recent decades, a future scenario that assumes continued accumulation of atmospheric greenhouse gases exhibited an increased frequency of WWEs, especially in cases when a persistent pattern of anomalous high-latitude warmth occurred, which is also a widely anticipated response to greenhouse warming.

In this new study, we apply the same approach to a different sector of the Northern Hemisphere—the region encompassing the North Atlantic Ocean and Europe—to investigate the past and

future behavior of continental-scale WWEs, as well as the extreme temperatures and precipitation associated with them.

RESULTS

Mean patterns and changing frequencies of occurrence

The characteristic patterns in 500 hPa height anomalies across the domain for all months are displayed in the master SOM matrix (Fig. 1). It is apparent that adjacent nodes are most similar to each other while those farthest apart are most dissimilar. Percentages over each map indicate the frequency with which a pattern occurs during winter (summer). Winter days are more numerous in patterns with large height contrasts spatially, while summer days are fairly evenly distributed across the SOM, meaning that none of the 12 patterns is substantially more common than another.

Patterns in the upper-left and lower-right part of the matrix feature zonal height anomalies with opposite signs: warm Arctic (anomalous ridging) in the upper left and cold Arctic (troughing) in the lower right. The dominant feature of patterns in the upper-right and lower-left corners is high-amplitude waves (meridional pattern), again with opposite signs. Stronger-than-normal ridging over Scandinavia would be expected during days belonging in nodes #3 and #4, while days belonging in nodes #5, #6, #9, and #10 would likely exhibit relatively strong ridging in the vicinity of Greenland.

Other variables corresponding to each day in the data set can be mapped onto the SOM nodes to elucidate relationships among quantities associated with each representative pattern. The corresponding daily sea-level pressure (SLP) fields belonging in each node are averaged and presented in Fig. 2. The predominantly barotropic nature of the atmosphere is evident in the similarity of patterns in 500 hPa height anomalies to the features

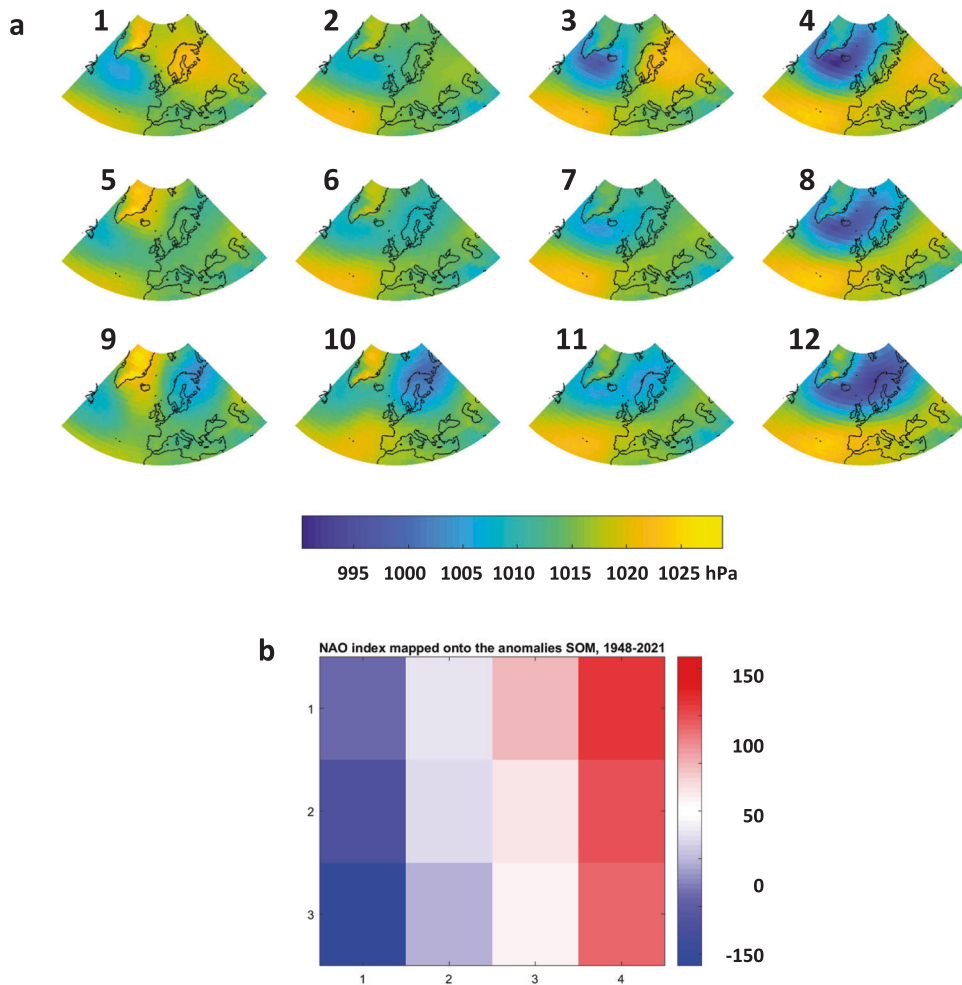


Fig. 2 Sea-level pressures and NAO index corresponding to the SOM. **a** Sea-level pressure (hPa) associated with each pattern in the master SOM (Fig. 1), averaged over all days belonging in a node. **b** North Atlantic Oscillation (NAO) index (unitless) averaged over all days in each node. Numbers on left and bottom of matrix indicate row and column number.

in SLP fields. Also shown in Fig. 2 is the corresponding North Atlantic Oscillation (NAO) index¹⁹ averaged over all days in each node. As expected, patterns with relatively low pressure in the North Atlantic along with high pressure in midlatitudes (nodes along the right side of the matrix) are reflected in a positive NAO index, while negative NAO values occur in nodes along the left side, where patterns feature high pressure in the northern part of the domain along with relatively low pressure to the south. A positive winter NAO index (right-side nodes) is generally associated with warmer, stormier conditions in northern Europe along with drier, cooler conditions in southern Europe. A positive NAO can also be associated with blocking over Europe²⁰, which can lead to European heat waves. A negative NAO (left-side nodes) typically brings the opposite conditions¹⁹.

Corresponding 2-meter air temperature anomalies are displayed in Fig. 3. Nodes along the left edge of the SOM feature strong positive anomalies over and near Greenland with negative anomalies dominating western and northern Europe. Clusters in the right column feature abnormally cool conditions over Greenland along with above-normal temperatures across much of Europe. High latitudes are unusually warm and low latitudes cool on days in node #3, with a nearly opposite pattern in node #10. These patterns in near-surface temperature anomalies are generally consistent with the circulation associated with 500 hPa height anomalies in Fig. 1 and SLP anomalies presented in Fig. 2.

Knowledge of which days belong in each node allows a calculation of changes in the frequency of occurrence of each pattern. Figure 4 presents the changes in frequency annually and for winter and summer seasons from a 20-year period during the early part of the record (1950–1969) to recent years (2002–2021). The changes paint a generally consistent picture all year, suggesting an overall increase in patterns featuring positive height anomalies over the Arctic (amplified Arctic warming) and a decrease in patterns with low heights over the Arctic. Annually, nodes #1 and #3 exhibit significant increases in frequency – patterns dominated by low SLP in the N. Atlantic Ocean with high pressure over northeastern Europe—and decreased frequencies of nodes #10 and #11, which feature high-pressure west of Portugal and low pressure over northern Europe. During winter months the frequencies of nodes #3 and #12 increase, both of which feature low pressure near Iceland and high pressure near the Azores, consistent with a positive NAO index. Nodes #9 and #10 have decreased in frequency, exhibiting relatively high-amplitude height anomalies with ridging over Greenland and troughing over western Europe. During summer months node #3 occurred more frequently—featuring abnormally warm temperatures across the Greenland-Iceland-Norwegian Seas—while node #11, with cool temperatures in high latitudes, occurred less frequently.

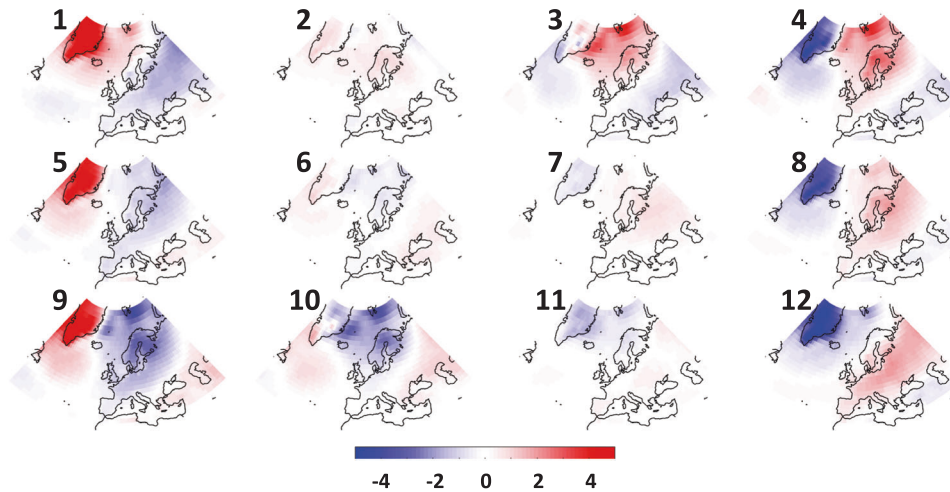


Fig. 3 Two-meter air temperature anomalies corresponding to the SOM. Two-meter air temperature anomalies (C) associated with each pattern in the master SOM (Fig. 1), averaged over all days belonging in a node.

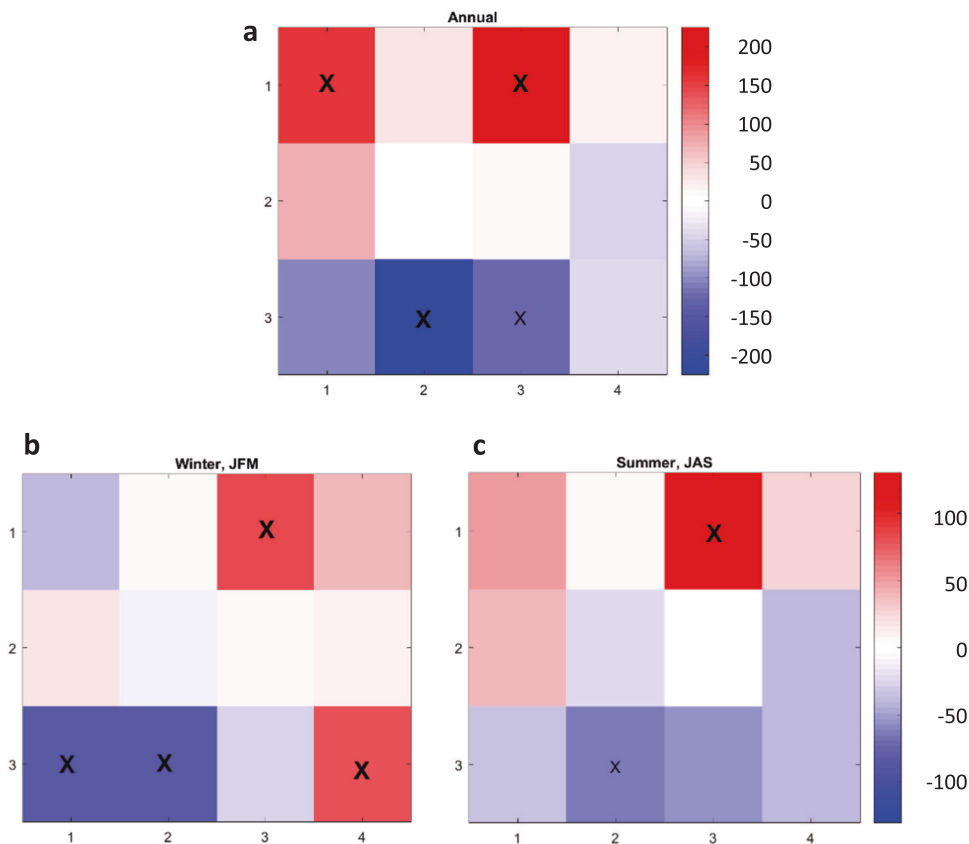


Fig. 4 Frequency changes in SOM nodes. Change in the frequency of occurrence (days) of each node from 1950–1969 to 2002–2021 during **a** all months, **b** winter (JFM), and **c** summer (JAS) based on NCEP reanalysis data. The small (large) Xs indicate changes that are statistically significant with 90% (95%) confidence using a student's-t test.

Recent changes in extremes

These changes in pattern frequency can be used to interpret the behavior of extreme temperature and precipitation associated with each pattern in the SOM. Figures 5, and 6 present node-averaged temperatures at 925 hPa exceeding 1.5σ on each day relative to the mean on that date (extreme heat), the same for temperatures below -1.5σ (extreme cold), and precipitation exceeding 1.5σ (heavy precipitation). The figures display the number of winter and summer days with extreme conditions. The

observed increased JAS frequency of node #3 during winter (Fig. 5) corresponds with more frequent abnormally warm days in the Greenland Sea along with more extreme cold conditions over much of the N. Atlantic and Europe. A higher number of heavy precipitation days is exhibited throughout the N. Atlantic, the Greenland Sea, and across the Mediterranean, consistent with predominantly low pressure in those areas (Fig. 2). The increased occurrence of node #12 would dictate a nearly opposite pattern of extremes. The decreased frequencies of nodes #9 and #10 suggest

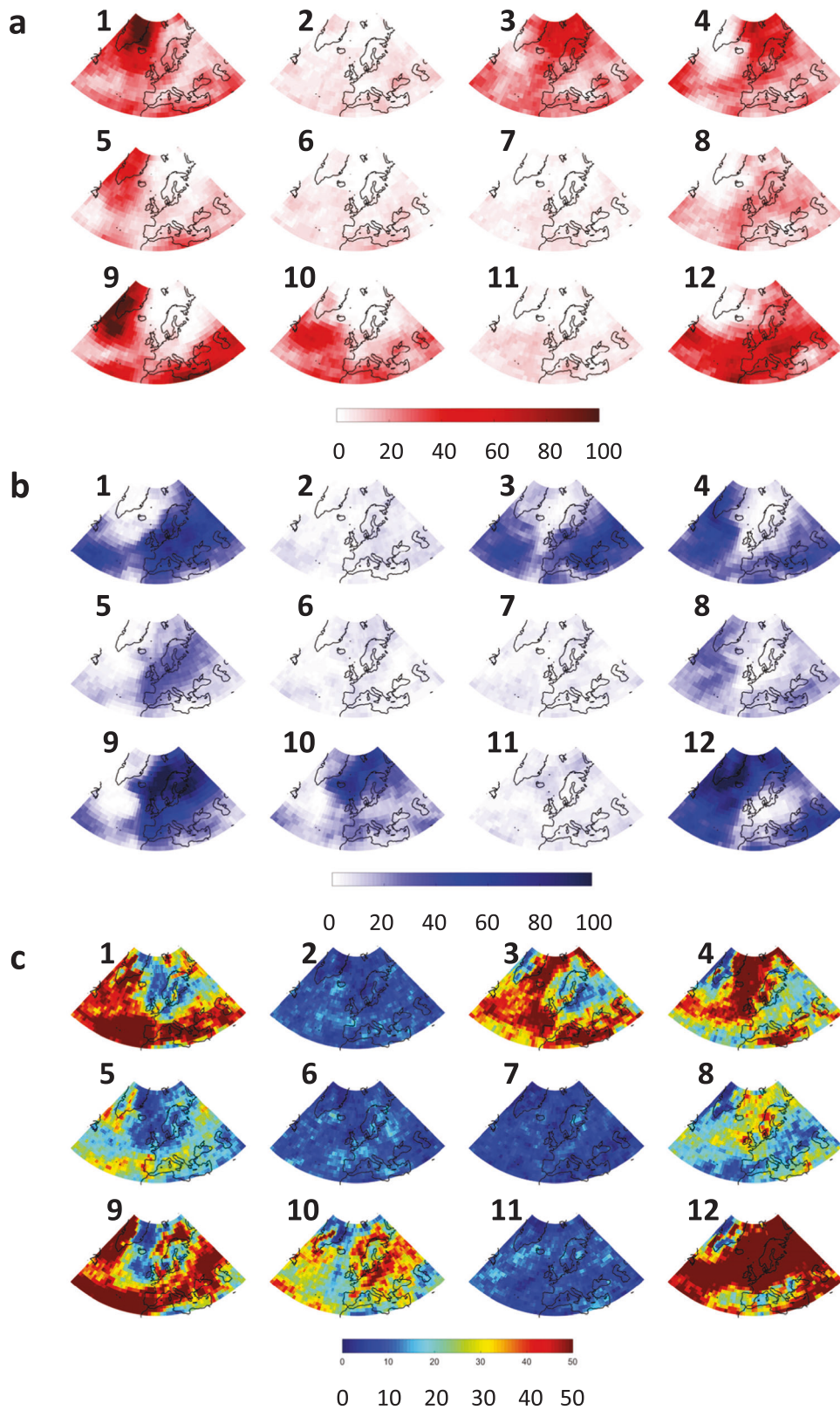


Fig. 5 Winter temperature and precipitation extremes associated with SOM nodes. Winter (JFM) temperature and precipitation extremes associated with each node of the master SOM. **a** Number of days (shading) that air temperature anomalies at 925 hPa exceed 1.5σ . **b** Same as **a** but for anomalies below -1.5σ . **c** Same as **a** but for daily precipitation anomalies exceeding 1.5σ . Data are from the NCEP/NCAR reanalysis.

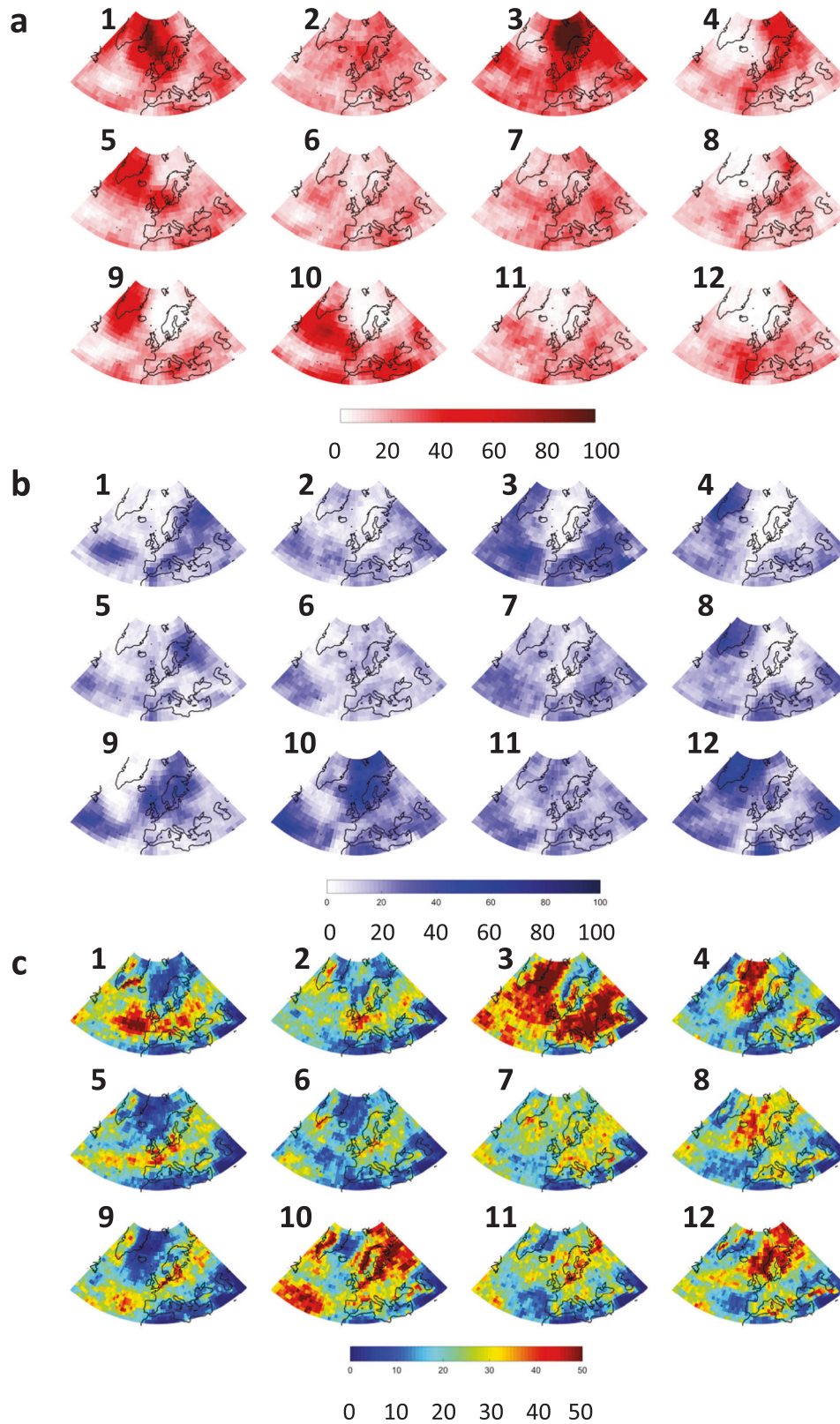


Fig. 6 Summer temperature and precipitation extremes associated with SOM nodes. Summer (JAS) temperature and precipitation extremes associated with each node of the master SOM. **a** Number of days (shading) that air temperature anomalies at 925 hPa exceed 1.5σ . **b** Same as **a** but for anomalies below -1.5σ . **c** Same as **a** but for daily precipitation anomalies exceeding 1.5σ . Data are from the NCEP/NCAR reanalysis.

fewer days with extreme heat over the N. Atlantic and Greenland and fewer extremely cold days over northern Europe and the Greenland Sea. Fewer days with extreme precipitation would occur over Greenland and midlatitudes of the domain. During summer months (Fig. 6), the repercussions of an increased frequency of node #3 are similar to those in winter. The decrease in node #11 corresponds with fewer abnormally hot days in midlatitudes of the domain, while the impacts on cool days and heavy precipitation is less distinct.

The observed frequency of WWEs and their temporal changes

Our objective method of assessing WWEs begins with the identification of long-duration events (LDEs) in reanalysis fields. Significant increasing trends in LDEs exist in nodes #1, #3, and #5, while node #10 exhibits declining trends (Supplementary Fig. 2). These findings are consistent with our earlier work on weather-regime persistence^{21–23}. Specifically, (21) found an increased occurrence of LDEs particularly in patterns featuring positive height anomalies in high latitudes. Increased LDEs in warm-Arctic nodes would favor more persistent weather conditions that can lead to extreme weather events.

The matrix of time series shown in Fig. 7a displays the frequency (events per year) with which a WWE originates from an LDE in each node. Our analysis produces a total of 1029 (annual), 255 (winter), and 235 (summer) WWEs over the 74-year record, which translates to an annual- or seasonal-mean frequency of 14, 3.4, and 3.2. These events are relatively rare because LDEs themselves occur infrequently^{1,21,22}. The rarity of WWEs along with a large interannual variability challenge the detection of frequency changes over the observational record, but a few nodes exhibit statistically significant trends. Nodes #1 and #12 initiate substantially more WWEs than do other nodes. Positive trends (albeit statistically insignificant) are evident for nodes #3 and #9, while node #10 exhibits a significant negative trend. The upward trends in nodes #3 and #9 are consistent with observed increased frequencies of blocking over Europe²⁴ and Greenland^{25,26}.

To illustrate changes in surface weather conditions corresponding with WWEs, we present two case studies in Supplementary Figs. 4, and 5; one case during February 1948 (pattern shift from node #8 to node #1) and another during September 2019 (pattern shift from node #9 to node #1). Fields of SLP anomalies, 2-m temperature anomalies, and daily mean precipitation rates are presented in Supplementary Fig. 4 for the mean during the preceding LDE and for the WWE two days later. Supplementary Fig. 5 displays the change in 2-meter air temperatures during the WWEs.

Case 1 exhibits a substantial shift in SLP: anomalously low pressure over the Greenland Sea and northwestern Europe is replaced with high pressure, and strong low pressure invades the northwest Atlantic. This shift is accompanied by substantially warmer temperatures over Greenland and colder temperatures from the central Mediterranean northward into western Russia. Heavy precipitation spreads into the northwest Atlantic along with dry conditions in the northeast Atlantic and Greenland Sea. During the second WWE case, substantial pressure falls occur over Greenland and the U.K. along with rises over eastern Scandinavia. This WWE brings strong warming to Greenland along with more negative temperature anomalies to western Russia. Heavy precipitation departs the Iberian Peninsula and moves into northern Mediterranean countries.

Figures 7b, c display the change in WWEs during winter (Fig. 7b) and summer (Fig. 7c) from a 20-year period in the early part of the data record (1950–1969) to the latest two decades (2002–2021). Node #4, featuring a high-amplitude pattern with anomalously high heights over northern Europe, is the only node with a significant increase in WWEs during winter. This pattern also features the highest frequency of blocking in the domain^{27,28} as well as the longest durations. High-amplitude jet-stream waves

tend to progress slowly and are often associated with persistent weather patterns.

A winter WWE originating in node #4 is most likely to shift to node #12 (Fig. 8a), a distinctly more zonal pattern with anomalously low heights in high latitudes. This regime shift would correspond with increased winter heat waves across southern Europe, more cold extremes in the Greenland Sea, and a higher likelihood of heavy precipitation days across the northern two-thirds of Europe (Figs. 3, 5). Warmer, drier conditions in the Mediterranean region are consistent with observations from recent decades²⁹. Fewer winter WWEs occurred in nodes #1, #9, and #10. During summer months, a significant increase in WWEs originating in node #3 is exhibited, which are most likely to shift to node #1 (Fig. 8b). Node #3 is a high-amplitude pattern with positive height anomalies over Scandinavia and low anomalies over Greenland. The shift to node #1 becomes a more zonal pattern with positive height anomalies across high latitudes along with negative anomalies in midlatitudes.

Model-simulated WWEs, past and future

One of the advantages of the SOM tool is that any gridded data can be mapped onto the master pattern matrix. We now analyze model-simulated 500 hPa height anomaly fields to identify WWEs in the historical period (1979–2005) to assess the model's ability to capture past WWE frequency and changes, and then we use future projections to assess changes in WWEs under the business-as-usual scenario (RCP 8.5) of climate forcing. WWEs identified in historical periods from 1979–1989 to 1995–2005 in both reanalysis output and 10 ensemble members from CESM are compared in Supplementary Fig. 3 for winter and summer. While the magnitudes of changes differ between the model runs and the reanalysis, the signs of changes are generally similar, lending confidence in the model's ability to appropriately capture WWEs. Given the large interannual variability in WWEs and the fact that the 1995–2005 period is relatively early in the era of the climate-change signal generally and the emergence of AAW specifically, it is not surprising that changes over two relative short periods do not align perfectly.

Changes in WWEs in future decades are presented in Fig. 9. From near present (2006–2030) to the end of the century (2076–2100), the CESM model indicates increased WWEs in patterns in the top row of the SOM matrix (particularly nodes #1 and #3) and a decreased occurrence in patterns along the bottom row (nodes #10, #11, and #12). The two seasons are similar, albeit more significant changes occur in the summer months. Nodes in the top row generally exhibit positive height anomalies in high latitudes, indicating that more WWEs will be initiated in circulation patterns exhibiting amplified Arctic warming, which are generally increasing in frequency. This result suggests that when the eastern Arctic is particularly warm and/or when blocking occurs over Scandinavia, WWEs are more likely to be initiated. Nodes in the bottom row feature anomalously negative height anomalies, suggesting fewer WWEs will occur in patterns with below-normal Arctic temperatures.

These changes in WWEs are clearly associated with trends in the frequency of long-duration events, displayed in Fig. 10. Model-simulated trends in LDEs are consistent with those derived from reanalysis data (Supplementary Fig. 2), lending further confidence to the model results. The nodes exhibiting an increased number of WWEs by the end of the century are the same as those indicating an increasing frequency of LDEs. The opposite is true for nodes with negative trends in LDEs. These results suggest the large-scale patterns associated with positive height anomalies in the Greenland-Iceland-Norwegian (GIN) Sea and Barents Sea, the region of the globe where observed warming trends are largest³⁰, will exhibit an increased number of persistent weather regimes as the globe continues to warm, which will also spawn an increase in WWEs.

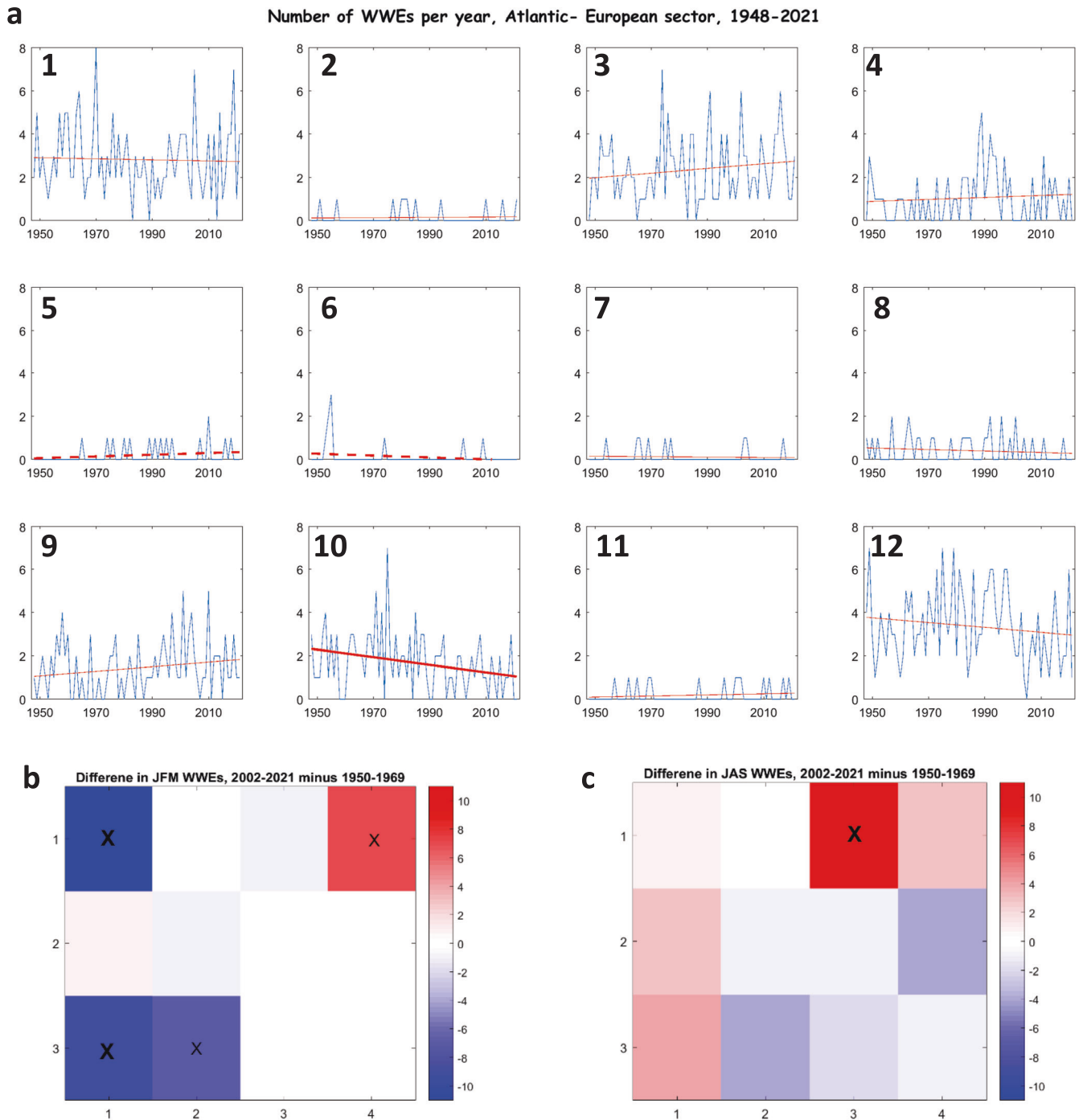


Fig. 7 **WWEs per year and changes.** **a** Time series of WWEs per year from 1950 to 2021. Solid (dashed) red lines indicate trends at 95% (90%) confidence based on a student's t-test. Change in total number of WWEs from 1950–1969 to 2002–2021 in winter (**b**) and summer (**c**). Large (small) Xs indicate significance at 95% (90%) confidence based on an f-test.

DISCUSSION

Our objective in this paper is to apply an objective approach¹ to identify and track the occurrence of seasonal weather whiplash events (WWEs) over the North Atlantic/European region, determine which large-scale atmospheric patterns are more or less likely to initiate them, assess extreme weather conditions associated with the patterns before and after a WWE, and measure frequency changes in past observations as well as in future projections as greenhouse gas concentrations continue to rise.

We define WWEs as abrupt shifts from one persistent, continental-scale weather regime to another substantially different pattern. These rapid transitions are often disruptive to agriculture, management of municipal utilities, animal behavior, and a variety of human activities. Characteristic patterns are objectively determined from 74 years of daily 500 hPa height anomaly fields, and each day is classified into a matrix of representative clusters or nodes by a neural-network-based tool called self-organizing maps. A long-duration event (LDE) is identified when a string of four or more consecutive days occurs in a single node of the matrix. A WWE is then diagnosed when the pattern two days following an LDE transitions to a pattern that is

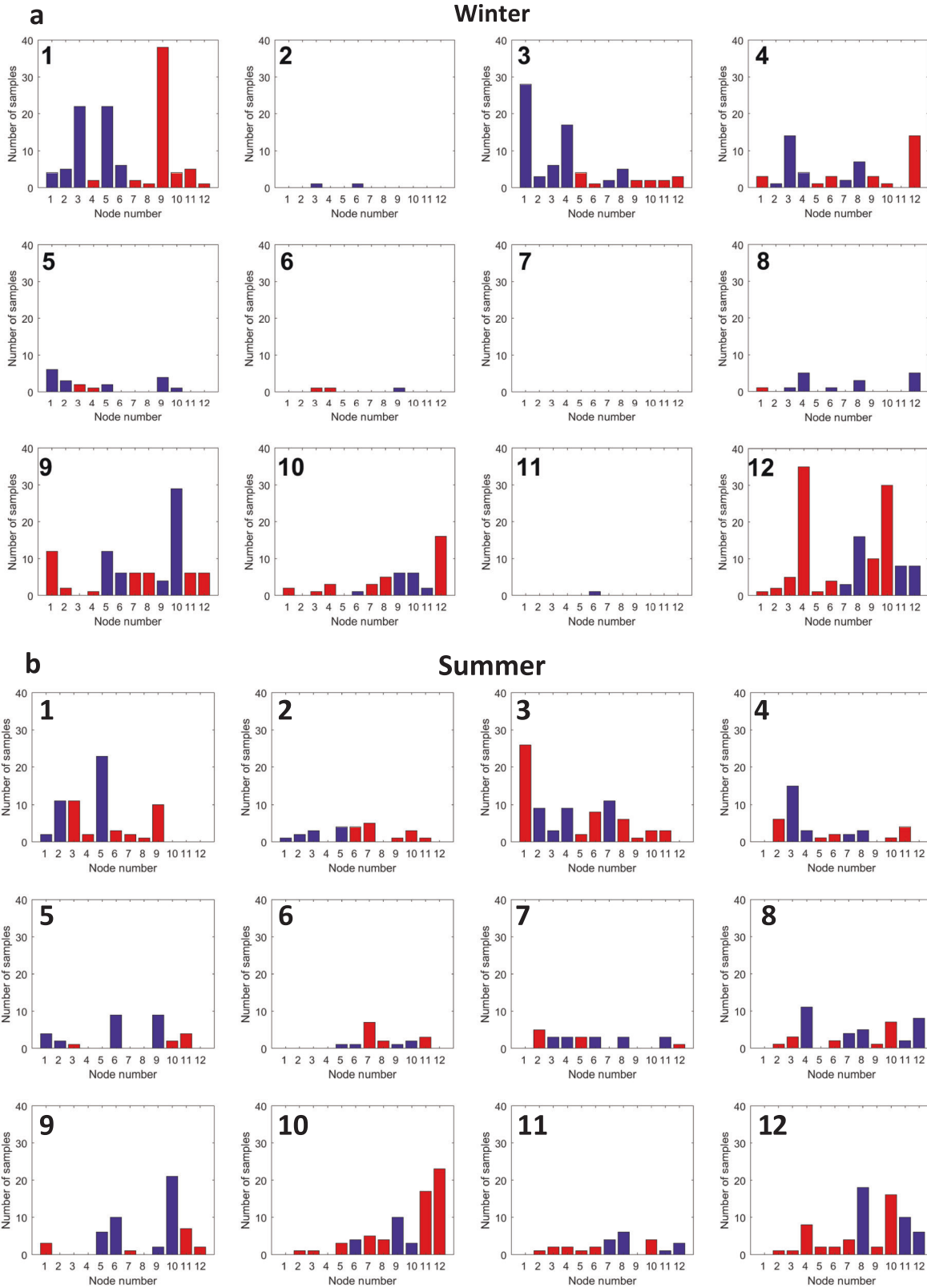


Fig. 8 Identification of patterns after WWEs. Distributions of days (y-axis) of node number (1–12, x-axis) corresponding to two days following a long-duration event (LDE) in a particular node during winter (a) and summer (b). The matrix corresponds to node placement in the master SOM shown in Fig. 1, indicated with bold numbers in the upper left corners. Red bars denote shifts that exceed the distance threshold and thus constitute a WWE; blue bars are non-WWEs.

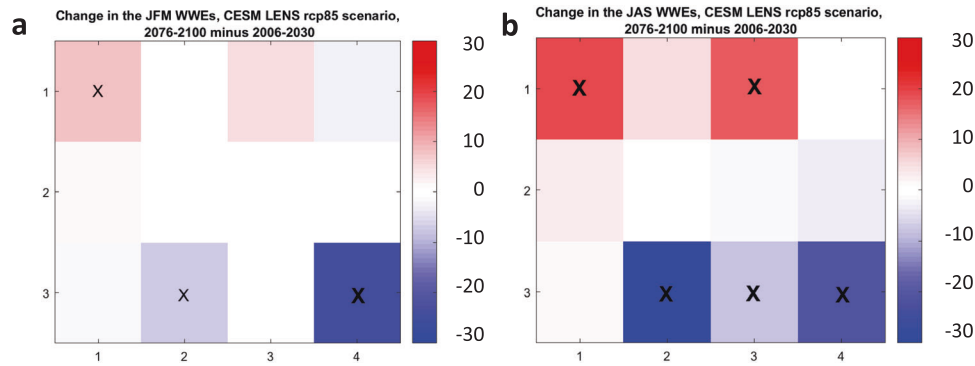


Fig. 9 Future changes in WWEs. Projected changes in the total number of WWEs from 2006–2030 to 2076–2100 in **a** winter and **b** summer based on ten simulations by CESM assuming RCP 8.5 forcing. Bold (normal) Xs indicate statistical significance > 95% (>90%) based on a student's t-test.

Trend in LDEs for CESM-LENS ensemble, rcp8.5 scenario, 2006–2100

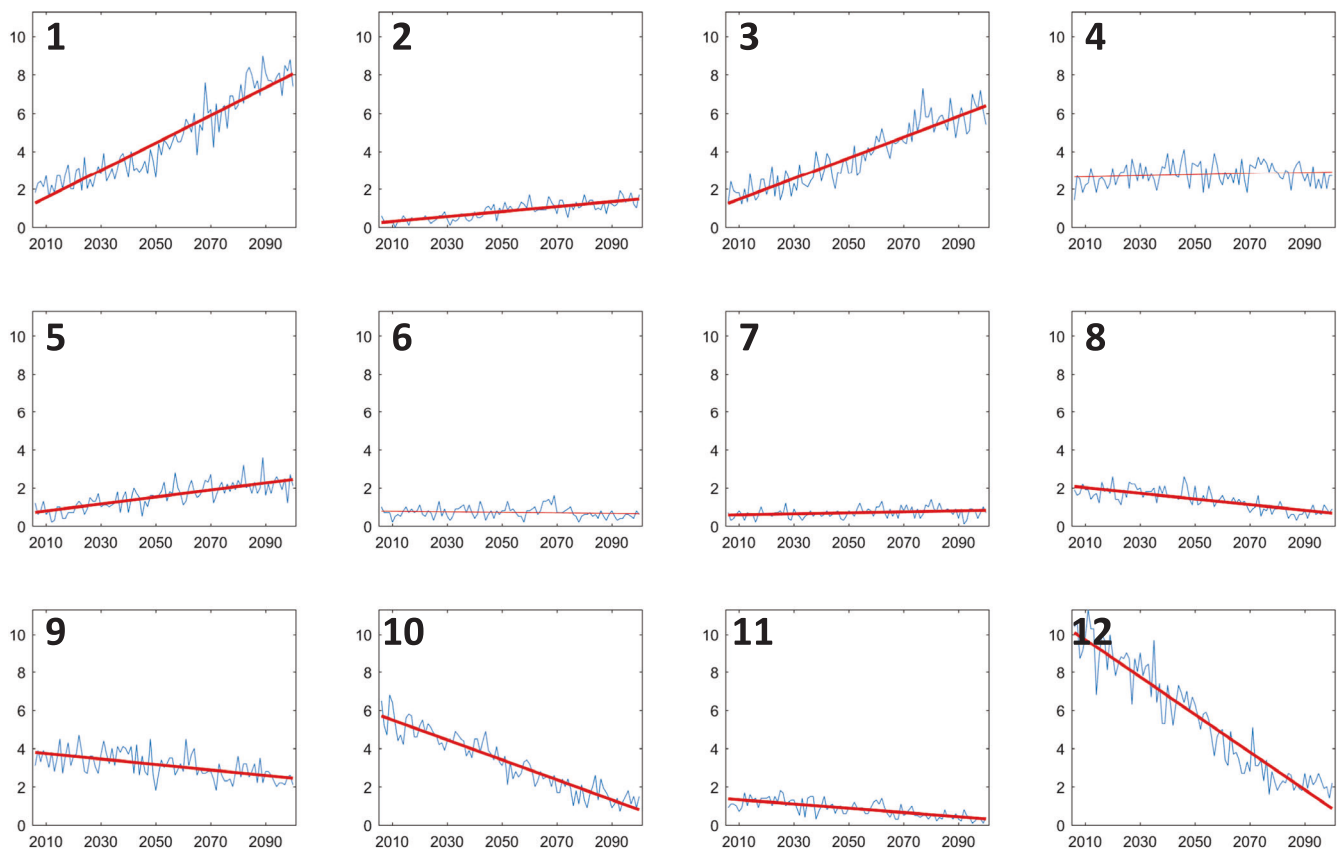


Fig. 10 Future trends in LDEs. Trends in the frequency (days yr^{-1}) of LDEs occurring in each node from 2006 to 2100 as projected by 10 ensemble members of the CESM-LENS model, assuming forcing conditions dictated by the RCP 8.5 scenario. Bold (thin) red lines indicate significant trends with a 95% (90%) confidence according to a student's t-test.

sufficiently different from the one where the LDE occurred, as measured by the Euclidean distance between nodes. Extreme temperatures and heavy precipitation associated with each pattern in the matrix are also characterized. This information is used to describe the expected shift in weather conditions before and after a WWE. Below is a summary of our main findings:

- Self-organizing maps appear to be an effective tool for assessing abrupt, continental-scale shifts in circulation regimes associated with weather whiplash events and disruptive transitions in weather conditions.
- WWEs originating in nodes featuring positive height anomalies over the GIN and Barents Seas, where observed warming has been largest, have become more frequent as the globe continues to warm, particularly during summer. WWEs have decreased in nodes exhibiting abnormally low heights in high latitudes. These nodes are also occurring less frequently, consistent with amplified Arctic warming.
- Abrupt regime transitions are associated with regional shifts in extremely high and low temperatures as well as heavy precipitation. These shifts are known to be disruptive to ecosystems and human activities.

- Changes exhibited in model projections for a warmer future are consistent with those in reanalysis output but are more robust.
- Nodes with projected increases in WWEs also exhibit increasing LDEs, suggesting higher likelihoods of persistent weather regimes that often cause extreme events.
- Projected changes in WWE frequency occur in the same nodes for the winter and summer months, with larger trends in summer.

These findings lead us to conclude that weather whiplash events in the North Atlantic/European region are likely to increase in frequency as the globe continues to warm in response to higher concentrations of greenhouse gases. Atmospheric patterns with enhanced warming in high latitudes, particularly those exhibiting positive height anomalies in high latitudes, are most likely to both increase in frequency and to spawn more WWEs, especially in summer. These findings are consistent with increasing trends in high-latitude blocking^{26–28}.

We now focus on the summer season (because trends during winter are weak) to describe the extreme weather transitions likely to be experienced with the increasing frequencies of WWE in nodes #1 and #3. A WWE initiated in node #1 would begin with long-duration weather conditions characterized by a high likelihood of abnormally warm temperatures over northwest Europe, Iceland, and northeast Greenland along with below-normal temperatures elsewhere in the domain (Fig. 6a, b). Heavy precipitation would be likely from the middle latitudes of the North Atlantic Ocean eastward across central Europe (Fig. 6c). WWEs initiated node #1 are most likely to shift to node #3 or node #9. In the case of node #3, the heat wave moves eastward to Scandinavia and the Barents Sea area, abnormally low temperatures invade Greenland, and the area prone to heavy precipitation shifts northward into the GIN Seas. Central Europe and the Mediterranean would also experience an increased frequency of heavy precipitation events. If instead the WWE flips to node #9, the heat wave engulfs Greenland, accompanied by a high chance for much-below-normal temperatures across most of northern Europe. The region of heavy precipitation in the North Atlantic weakens, while the band over Europe shifts northward. The other node exhibiting an increased frequency of WWE initiation is node #3. The long-duration conditions associated with this pattern are above-normal temperatures over the GIN Seas and below-normal temperatures elsewhere in the domain. A high likelihood of heavy precipitation also spans the GIN Seas as well as across central and southern Europe. From node #3 the WWE is most likely to shift to node #1, which moves the heat wave westward from Scandinavia to east Greenland and Iceland and reduces the likelihood of heavy precipitation over central Europe and the GIN Seas.

Future efforts will examine WWEs in other sectors of the globe and further investigate relationships between WWE frequency and human-caused changes in the climate system, such as rapid Arctic warming, disruptions of the stratospheric polar vortex, and oceanic heat waves. These relationships may differ during varying phases of natural climate oscillations, such as El Niño/La Niña and the Pacific Decadal Oscillation. Because WWEs tend to cause abrupt and disruptive shifts in weather conditions, a better understanding of these events – and the extremes associated with them – will better enable preparations by decision-makers, farmers, utilities, and the general public that will lessen the impacts of these abrupt shifts in weather regimes.

METHODS

Self-organizing maps (SOMs)

At the heart of this analysis is the Self Organizing Maps tool, a neural-network-based algorithm that identifies patterns in large sets of two-dimensional data, which in this case are daily maps of 500 hPa height

anomalies in the domain bounded by 30°N–80°N and 60°W–60°E. Because the approach in this study applies that used in F22 for the North American/North Pacific longitude sector, only a brief description will be provided here. Please see F22 for further details.

The SOM algorithm ingests large, two-dimensional data sets and groups the fields into clusters or nodes of representative patterns found in the data. The patterns are arranged in a variable-size matrix according to their similarity with each other, with most similar patterns positioned near each other and most dissimilar patterns farthest apart. For this application, we use daily fields of anomalies in the 500-hPa geopotential heights from 1948–2021 (~27,000 days) obtained from the National Center for Environmental Prediction/National Center for Atmospheric Research (NCEP/NCAR) Reanalysis³¹. This should cite Kalnay et al While newer reanalysis products are available, it has been shown that large-scale, upper-level height fields are consistent across reanalyses³², and the relatively coarse resolution of this data set is more compatible with that of global climate models. Daily anomalies were calculated by subtracting the 74-year mean value for each gridpoint for that calendar day.

For this application, we chose a 4×3 SOM matrix, which balances sufficient representation of the atmosphere's dominant patterns with ease of displaying results (Fig. 1). Through an iterative process based on a neural network, the algorithm places each daily field into the node with the most similar pattern (See F22 for further details). Once this so-called master SOM has been created, other fields of data can be mapped to the patterns, which is especially powerful for variables that are spatially and/or temporally discontinuous (e.g., cloud cover, precipitation, or temperature). We take advantage of this tool to explore surface pressure as well as extreme temperatures and precipitation associated with each pattern. Changing frequencies of occurrence of each SOM node allow an assessment of trends in variables associated with the large-scale patterns. Sea-level pressure, air temperature at 925 hPa, and precipitation data are also obtained from the NCEP/NCAR Reanalysis. While precipitation data are never perfect, daily-mean values at the grid-box scale (2.5°) should reasonably represent coherent patterns and their changes over time.

Identification of weather whiplash events (WWEs)

WWEs are identified by first finding long-duration events (LDEs), defined as cases when the large-scale atmospheric pattern remains in one node of the SOM for four or more consecutive days^{1,21–23}. We then identify the node associated with the second day after each LDE during winter (January–March) and summer (July–September), then determine the Euclidean distance between the node exhibiting the LDE and the one for the atmospheric pattern two days later as a measure of dissimilarity between the patterns. When that dissimilarity is sufficiently large (see below for selection criteria for seasonal thresholds), the shift is considered a WWE. In practical terms, a WWE is experienced when a persistent weather pattern ends abruptly and it is replaced by weather conditions that differ markedly from the prior regime.

We compiled the distribution of Euclidean distances from each LDE (about 2,180 of them from 1948 to 2021) to the node containing the pattern two days later and determined that the 50th percentile distance value establishes a suitable threshold for identifying a WWE. Supplementary Table 1 displays these results for winter. The threshold value (i.e., 50th percentile) corresponds to a mean Euclidean distance of 1546 m (a metric internal to the SOM algorithm), and thereby constitutes a substantial pattern shift (e.g., from #1 to #9, Supplementary Table 2). For summer months, this threshold is 941, consistent with reduced pattern contrasts in the warm season when the jet stream is farther poleward and north-south temperature gradients are generally smaller. We then identify a WWE when the distance from the LDE node to the node

two days later exceeds the seasonal threshold, which also enables us to quantify the WWE magnitude by the amount of threshold exceedance.

Further insight into this methodology is illustrated in Fig. 8. The bar charts display the node number containing the sample that occurs two days after a winter LDE originating in each node in the matrix (the same approach was also applied to summer cases). For example, the top left chart indicates that the samples two days after LDEs occurring in node #1 shift most frequently to node #9, followed by #3 and #5. Note that when the same node number as that of the initiating LDE appears in the bar chart—e.g., the chart for node #1 has a bar for node #1—it means that the pattern shifted away from node #1 on the first day then returned to node #1 on the 2nd day. An additional visualization of the Euclidean distances between nodes is presented in Supplementary Fig. 1, a so-called Sammon map of the SOM matrix. The uneven distribution of distances between nodes is evident, and this mapping shows that nodes in opposing corners exhibit the largest differences among the circulation patterns.

The same methodology for identifying WWEs in reanalysis output was also applied to output from climate model simulations. We analyzed ten ensemble members from the NCAR Community Earth System Model Large Ensemble (CESM1) that span the historical period (1979–2005) as well as into the future (2006–2100)³³. Daily 500 hPa height fields were obtained from <https://www.cesm.ucar.edu/projects/community-projects/MMLEA/>. Historical runs incorporate observed natural and anthropogenic forcings, while future projections assume conditions defined by the representative concentration pathway (RCP) 8.5 scenario³⁴. Anomalies in future projections were calculated relative to the mean from 2006 to 2100.

North Atlantic Oscillation (NAO) index

The North Atlantic Oscillation index was calculated as the difference in the normalized sea-level pressure anomalies between Ponta Delgada, Azores and Reykjavik, Iceland. More information about the methodology is available from https://www.cpc.ncep.noaa.gov/products/precip/CWlink/pna/nao_index.html.

DATA AVAILABILITY

Reanalysis data used in this study are described in Kalnay et al.³¹ and are available from (<https://psl.noaa.gov/data/gridded/data.ncep.reanalysis.pressure.html>). Model simulations used in this study were obtained from <https://www.cesm.ucar.edu/projects/community-projects/MMLEA/> and are described in Kay et al. and Riahi et al.^{33,34}. No data sets were created as a part of this investigation.

CODE AVAILABILITY

The code used to calculate self-organizing maps was obtained from <http://www.cis.hut.fi/somtoolbox/>.

Received: 13 July 2023; Accepted: 6 December 2023;

Published online: 21 December 2023

REFERENCES

- Francis, J. A., Skific, N., Vavrus, S. J. & Cohen, J. Measuring “weather whiplash” events in North America: A new large-scale regime approach. *J. Geophys. Res. Atmos.* **127**, e2022JD036717 (2022).
- Copernicus Climate Change Service (C3S). European State of the Climate 2022, Summary: <https://doi.org/10.24381/gvaf-h066> (2023).
- Giannakopoulos, C., Kostopoulou, E., Varotsos, K. V., Tziotziou, K. & Palitharas, A. An integrated assessment of climate change impacts for Greece in the near future. *Reg. Environ. Change* **11**, 829–843 (2011).
- Zhang, R. et al. Increased European heat waves in recent decades in response to shrinking Arctic sea ice and Eurasian snow cover. *npj Clim. Atmos. Sci.* **3**, <https://doi.org/10.1038/s41612-020-0110-8> (2020).
- Christidis, N. & Stott, P. A. Human Influence on seasonal precipitation in Europe. *J. Clim.* **35**, 5215–5231 (2022).
- Schipanski, M. E. et al. Moving from measurement to governance of shared groundwater resources. *Nat. Water* **1**, 30–36 (2023).
- Webber, H. et al. Diverging importance of drought stress for maize and winter wheat in Europe. *Nat. Commun.* **9**, 42–49 (2018).
- Toreti, A., Bassu, S., Ceglar, A., & Zampieri, M. Climate change and crop yields. In P. Ferranti, J. R. Anderson, & E. M. Berry (Eds.), *Encyclopedia of food security and sustainability* (1, 223–227). Cambridge: Elsevier (2019).
- Turco, M. et al. On the key role of droughts in the dynamics of summer fires in Mediterranean Europe. *Sci. Rep.* **7**, 1–10 (2017).
- Angra, D. & Sapountzaki, K. Climate change affecting forest fire and flood risk—facts, predictions, and perceptions in Central and South Greece. *Sustainability* **14**, 13395 (2022).
- Cohen, J. An observational analysis: Tropical relative to Arctic influence on midlatitude weather in the era of Arctic amplification. *Geophys. Res. Lett.*, **43**, <https://doi.org/10.1002/2016GL069102> (2016).
- Lee, C. C. Weather whiplash: Trends in rapid temperature changes in a warming climate. *Int. J. Clim.*, 1–9 (2021).
- Park, H.-L., Seo, K.-H., Kim, B.-M. & Wang, S.-Y. S. Dominant wintertime surface air temperature modes in the Northern Hemisphere extratropics. *Clim. Dyn.* **56**, 687–698 (2021).
- Loecke, T. D. et al. Weather whiplash in agricultural regions drives deterioration of water quality. *Biogeochem* **133**, 7–15 (2017).
- Swain, D. L., Langenbrunner, B., Neelin, J. D. & Hall, A. Increasing precipitation volatility in twenty-first-century California. *Nat. Clim. Change* **8**, 427–433 (2018).
- He, X. & Sheffield, J. Lagged compound occurrence of droughts and pluvials globally over the past seven decades. *Geophys. Res. Lett.*, **47**, <https://doi.org/10.1029/2020GL087924> (2020).
- Kohonen, T. Learning Vector Quantization. In: *Self-Organizing Maps*. Springer Series in Information Sciences, **30**. Springer (2001).
- Skific, N. & Francis, J. A. “Self-Organizing Maps: A Powerful Tool for the Atmospheric Sciences” in *Applications of Self-Organizing Maps*, ISBN 978-953-51-0862-7, edited by M. Johnsson, <https://doi.org/10.5772/54299> (2012).
- Hurrell, J. W. Decadal trends in the North Atlantic Oscillation: Regional temperatures and precipitation. *Science* **269**, 676–679 (1995).
- Li, M. Y., et al. Collaborative impact of the NAO and atmospheric blocking on European heatwaves, with a focus on the hot summer of 2018. *Environ. Res. Lett.*, **15** <https://iopscience.iop.org/article/10.1088/1748-9326/aba6ad> (2020).
- Francis, J. A., Skific, N. & Vavrus, S. J. North American weather regimes are becoming more persistent: Is Arctic amplification a factor? *Geophys. Res. Lett.*, **45**, <https://doi.org/10.1029/2018GL080252> (2018).
- Francis, J. A., Skific, N. & Vavrus, S. J. Evidence for increased persistence of large-scale circulation regimes over Asia in the era of amplified Arctic warming, past and future. *Nat. Sci. Rep.*, **10**, <https://doi.org/10.1038/s41598-020-71945-4> (2020).
- Vihma, T. et al. Effects of the tropospheric large-scale circulation on European winter temperatures during the period of amplified Arctic warming. *Int. J. Clim.*, 1–21, <https://doi.org/10.1002/joc.6225> (2019).
- Rimbu, N. & Felis, T. On the relationship between Scandinavian extreme precipitation days, atmospheric blocking and Red Sea coral oxygen isotopes. *Environ. Res. Clim.*, **1**, <https://doi.org/10.1088/2752-5295/ac806b> (2022).
- Sellevoold, R., Lenaerts, J. T. M. & Vizcaino, M. Influence of Arctic sea-ice loss on the Greenland ice sheet climate. *Clim. Dyn.* **58**, 179–193 (2022).
- Preece, J. R. et al. Summer atmospheric circulation over Greenland in response to Arctic amplification and diminished spring snow cover. *Nat. Commun.* **14**, 3759 (2023).
- Luo, D., Zhang, W., Zhong, L. & Dai, A. A nonlinear theory of atmospheric blocking: a potential vorticity gradient view. *J. Atmos. Sci.* **76**, 2399–2427 (2019).
- Li, M., Luo, D., Simmonds, I., Yao, Y. & Zhong, L. Bidimensional climatology and trends of Northern Hemisphere blocking utilizing a new detection method. *Quart. J. R. Meteor. Soc.* **149**, 1932–1952 (2023).
- Tuel, A. & Eltahir, E. A. B. Why is the Mediterranean a climate change hot spot? *J. Clim.* **33**, 5829–5843 (2020).
- Rantanen, M. et al. The Arctic has warmed nearly four times faster than the globe since 1979. *Commun. Earth Environ.* **3**, 168 (2022).
- Kalnay, E. et al. The NCEP/NCAR 40-year Reanalysis project. *Bull. Am. Met. Soc.* **77**, 437–472 (1996).
- Archer, C. L., & Caldeira, K. Historical trends in the jet streams. *Geophys. Res. Lett.*, **35**, <https://doi.org/10.1029/2008GL033614> (2008).
- Kay, J. E. et al. The Community Earth System Model (CESM) Large Ensemble Project: A community resource for studying climate change in the presence of internal climate variability. *Bull. Am. Meteor. Soc.* **96**, 1333–1349 (2015).
- Riahi, K., et al. A scenario of comparatively high greenhouse gas emissions. *Clim. Change*, **109**, <https://doi.org/10.1007/s10584-011-0149-y> (2011).

ACKNOWLEDGEMENTS

J. Francis and N. Skific are grateful to the Fund for Climate Solutions at the Woodwell Climate Research Center for supporting this research. Contributions by Z. Zobel are supported by funding from the Woodwell Climate Research Center.

AUTHOR CONTRIBUTIONS

J.A.F. conceptualized the project, acquired the funding, oversaw the analysis, and wrote the original draft. N.S. performed the calculations, developed the visualizations, and contributed to the manuscript. Z.Z. contributed to the analysis and manuscript.

COMPETING INTERESTS

The authors declare no competing interests.

ADDITIONAL INFORMATION

Supplementary information The online version contains supplementary material available at <https://doi.org/10.1038/s41612-023-00542-9>.

Correspondence and requests for materials should be addressed to Jennifer A. Francis.

Reprints and permission information is available at <http://www.nature.com/reprints>

Publisher's note Springer Nature remains neutral with regard to jurisdictional claims in published maps and institutional affiliations.



Open Access This article is licensed under a Creative Commons Attribution 4.0 International License, which permits use, sharing, adaptation, distribution and reproduction in any medium or format, as long as you give appropriate credit to the original author(s) and the source, provide a link to the Creative Commons license, and indicate if changes were made. The images or other third party material in this article are included in the article's Creative Commons license, unless indicated otherwise in a credit line to the material. If material is not included in the article's Creative Commons license and your intended use is not permitted by statutory regulation or exceeds the permitted use, you will need to obtain permission directly from the copyright holder. To view a copy of this license, visit <http://creativecommons.org/licenses/by/4.0/>.

© The Author(s) 2023